ISSN 1001-0742
CN 11-2629/X

2012
Volume 24
Number 12

JOURNAL OF ENVIRONMENTAL SCIENCES

ELSEVIER
Science Press

Sponsored by
Research Center for Eco-Environmental Sciences
Chinese Academy of Sciences

ISSN 1001–0742 **Journal of Environmental Sciences** Vol. 24 No. 12 2012

CONTENTS

Serial parameter: CN 11-2629/X*1989*m*170*en*P*21*2012-12

Available online at www.sciencedirect.com
ScienceDirect
Journal of Environmental Sciences 2012, 24(12) 2083–2090
JOURNAL OF ENVIRONMENTAL SCIENCES
ISSN 1001-0742
CN 11-2629/X
www.jesc.ac.cn

Mercury oxidation and adsorption characteristics of potassium permanganate modified lignite semi-coke

Huawei Zhang*, Jitao Chen, Peng Liang, Li Wang

College of Chemical and Environmental Engineering, Shandong University of Science and Technology, Qingdao 266590, China. E-mail: sdkdzhw@163.com

Received 19 March 2012; revised 18 August 2012; accepted 31 August 2012

Abstract

The adsorption characteristics of virgin and potassium permanganate modified lignite semi-coke (SC) for gaseous Hg^0 were investigated in an attempt to produce more effective and lower price adsorbents for the control of elemental mercury emission. Brunauer-Emmett-Teller (BET) measurements, X-ray powder diffraction (XRD) and X-ray photoelectron spectroscopy (XPS) were used to analyze the surface physical and chemical properties of SC, Mn-SC and Mn-H-SC before and after mercury adsorption. The results indicated that potassium permanganate modification had significant influence on the properties of semi-coke, such as the specific surface area, pore structure and surface chemical functional groups. The mercury adsorption efficiency of modified semi-coke was lower than that of SC at low temperature, but much higher at high temperature. Amorphous Mn^{7+}, Mn^{6+} and Mn^{4+} on the surface of Mn-SC and Mn-H-SC were the active sites for oxidation and adsorption of gaseous Hg^0, which oxidized the elemental mercury into Hg^{2+} and captured it. Thermal treatment reduced the average oxidation degree of Mn^{x+} on the surface of Mn-SC from 3.80 to 3.46. However, due to the formation of amorphous MnO_x, the surface oxidation active sites for gaseous Hg^0 increased, which gave Mn-H-SC higher mercury adsorption efficiency than that of Mn-SC at high temperature.

Key words: lignite semi-coke; elemental mercury; potassium permanganate modification; removal efficiency

DOI: 10.1016/S1001-0742(11)61047-4

Introduction

Mercury is one of the most dangerous heavy metals for the environment and human beings. The techniques for mercury removal have been researched all over the world (Bolger and Szlag, 2002; Presto and Granite, 2006). According to the global mercury mass balance model, the total anthropogenic mercury emission was 1930 tons in 2010, of which coal burning accounts for 890 tons, about 46% of the total emissions (Sundseth et al., 2010; Pirrone et al., 2010).

The mercury concentration in flue gas is about 1–20 μg/m^3. Mercury in coal decomposes into its elemental form (Hg^0) through coal combustion. A portion of the elemental mercury is converted to oxidized forms (Hg^{2+}) and particulate-bound atoms (Hg_p), which can be captured effectively in wet scrubbers and electrostatic precipitators. However, it is difficult to remove gaseous Hg^0 due to its lack of solubility in water and stable thermodynamic properties. Nowadays, one of the most effective ways for gaseous Hg^0 removal is injecting varieties of solid adsorbents into flue gas, which can oxidize the elemental mercury into Hg^{2+} and capture it. Many studies have focused on the preparation of high efficiency, long-term effectiveness and low-price Hg^0 adsorbents. Activated carbon adsorbents modified by chlorine, bromine, iodine, sulfur and metal oxides display high Hg^0 removal efficiency, but they are too expensive for most power plants (Lee et al., 2004, 2009; Hutson et al., 2007; Hsi et al., 2001; Wang et al., 2010; Mei et al., 2008). Non-carbon adsorbents, such as zeolite, calcium-based sorbents and fly-ash are cheaper, but their Hg^0 removal efficiency is much lower (Jurng et al., 2002; Gatica and Vidal, 2010; Hower et al., 2010). Compared with common adsorbents, semi-coke has the properties of a well-developed pore structure, abundant surface functional groups and low price, and can be used as an ideal adsorbent in the fields of water treatment, oil product purification, desulfurization and denitrification of flue gas (Shangguan et al., 2005; Gálvez et al., 2008; Yuan et al., 2010).

In previous work, we reported the preparation of silver-loaded semi-coke and its adsorption characteristics toward gaseous Hg^0 (Zhang et al., 2011). This research investigated the Hg^0 removal efficiency of virgin and potassium permanganate-modified lignite semi-coke in a lab-scale fixed-bed system. The adsorption mechanism of Hg^0 on the surface of the adsorbent was also discussed.

* Corresponding author. E-mail: sdkdzhw@163.com

1 Experimental

1.1 Sample preparation

Lignite semi-coke was sourced from Huolinhe City, Neimeng Province, China. It was pyrolyzed in a muffle furnace at 700°C for 1 hr, after which it was cooled down to room temperature and crushed into powder (80 to100 mesh). This sample was named SC. SC (10 g) was impregnated in a potassium permanganate solution (0.06 mol/L), and stirred for 4 hr at 90°C in a water bath. The sample was filtered and dried after treatment, and was named Mn-SC. Considering that the decomposition point of potassium permanganate is 240°C, Mn-H-SC was obtained after the thermal treatment of Mn-SC at 260°C under N_2 protection for 1.5 hr. After the mercury adsorption experiments for 12 hr at 140°C, the samples of Mn-SC and Mn-H-SC were named Hg-Mn-SC and Hg-Mn-H-SC, respectively.

1.2 Characterization

Physical characterization of the samples was carried out by the Brunauer-Emmett-Teller (BET) method; the surface area and pore size distribution were obtained by adsorbing and desorbing in N_2 at 77 K using an automatic volumetric multipoint apparatus (SSA-4300, Builder, China). Before the measurement, all samples were outgassed at 100°C for 2 hr. The identification of crystalline phases was carried out using an X-ray powder diffractometer (Rigaku, D/max-2500/PC). The experimental conditions were as follows: accelerating voltage 40 kV, current 25 mA, X-ray filtered radiation Cu $K\alpha\lambda$ =1.54056 Å, step size 0.020 (2θ), counting time at every point, 2 sec. The diffraction pattern was collected in the range of 2θ (0–100°) at room temperature. X-ray photoelectron spectroscopy (Thermo ESCALAB 250) with Al $K\alpha$ ($h\nu$ = 1486.6 eV) as the excitation source was used to determine the binding energies of C1s, O1s, Mn2p and Hg4f. The C1s line at 284.6 eV was taken as a reference for the binding energy calibration.

1.3 Experimental methodology and instrumentation

As shown in Fig. 1, gaseous Hg^0 adsorption experiments were carried out in a fixed-bed reactor, which consisted of flue gas simulation, gas adsorption and tail gas analyzing equipment. A constant flow of high purity nitrogen passed through the mercury permeation tube (VICI Metronics) and yielded a stable concentration of gaseous Hg^0. An oil bath pot was employed to keep the quartz tube at the desired temperatures during the adsorption. The mercury concentration in the tail gas was measured online by a QM201H mercury analyzer.

A simulated flue gas stream with the required temperature and Hg^0 concentration was produced by a mercury permeation tube. The concentrations of mercury were adjusted by altering the temperatures of permeation and the fluxes of mercury-carrying gas. The diluted stream was fed to the reactor (ID 1.0 cm, length 15 cm) containing the adsorbent sample, which was kept in an oil bath for temperature control. Adsorbent particles (0.5 g) were mixed with 3.0–4.0 g inert glass beads with an adsorbent bed height of 1.2 cm. The gas flow rate was 1 L/min. The Hg^0 concentration in the inlet stream (C_0) was (35±2) μg/m^3 and the adsorption temperatures ranged from 30 to 140°C. The Hg^0 concentrations in the inlet (C_0) and outlet (C_t) stream were measured by the mercury analyzer. The waste tail gas was purified by passing through a solution of 10% H_2SO_4 and 4% $KMnO_4$ before being discharged. The result of mercury mass balance analysis (> 90%) indicated that the experimental system was reliable.

Penetration rate, mercury removal efficiency and mercury adsorption capacities are significant for adsorbent evaluation. For a given adsorbent, the lower the value of breakthrough, the better the mercury removal. Similarly, higher mercury removal efficiency and capacity means a good adsorbent for mercury capture (Jurng et al., 2002). The mercury removal efficiency (η) of an adsorbent sample toward gaseous Hg^0 can be calculated by Eq. (1):

$$\eta = 1 - C_t/C_0 \quad (1)$$

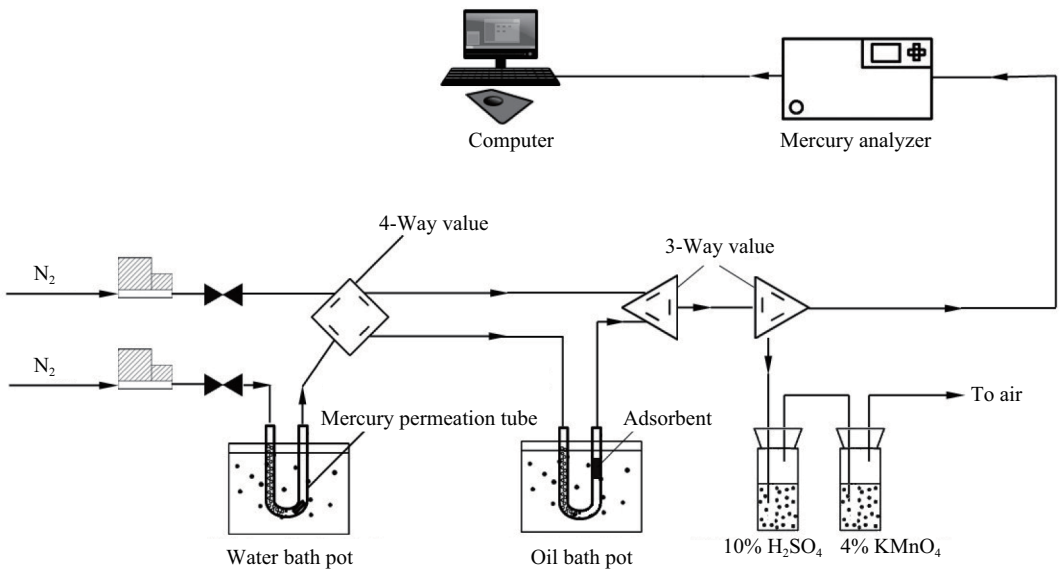

Fig. 1 Experimental device for adsorption of mercury.

Mercury adsorption capacity could be calculated by integrating the area under the removal curve within the reaction time.

2 Results and discussion

2.1 Specific surface area and pore structure

The BET results of SC, Mn-SC and Mn-H-SC are shown in Table 1 and Fig. 2. On the surface of sample SC, micropores accounted for 72.4% of the total pores. Potassium permanganate modification reduced the micropore content to 59.6% by filling the pores, which led to lower specific surface area and total pore volume capacity. After thermal treatment, the specific surface area and total pore volume capacity increased, and average pore size decreased, which indicated that the modification by thermal treatment opened the closed pores in Mn-SC. The micropore content of Mn-H-SC was less than those of SC and Mn-SC, which was 50.2%, but the total micropore volume capacity of the Mn-H-SC was higher than that of Mn-SC.

2.2 X-ray diffraction

When the concentration of potassium permanganate was 2 wt.%, only SiO_2 was detected by X-ray diffraction in the sample (Fig. 3). This indicated that MnO_x was highly dispersed on the surface of the semi-coke in the amorphous state (i.e., no crystalline MnO_x was detected). As the concentration of potassium permanganate increased to 10 wt.%, $KMnO_4$ could be detected easily. This meant that more than a monolayer amount had been loaded on the surface of the semi-coke, and some of it existed in the crystalline state. After the 10 wt.% Mn-SC was thermally treated at 260°C, no crystalline $KMnO_4$ could be detected. This result indicated that the crystalline $KMnO_4$ on the surface of the semi-coke decomposed into amorphous MnO_x.

Table 1 BET surface area and pore parameters of SC, Mn-SC and Mn-H-SC

Sample	Particle size (mm)	Specific surface area (m^2/g)	Total volume capacity (cm^3/g)	Average pore size (nm)
SC	0.12–0.15	84.203	0.107	2.55
Mn-SC	0.12–0.15	32.207	0.071	4.43
Mn-H-SC	0.12–0.15	65.494	0.120	3.67

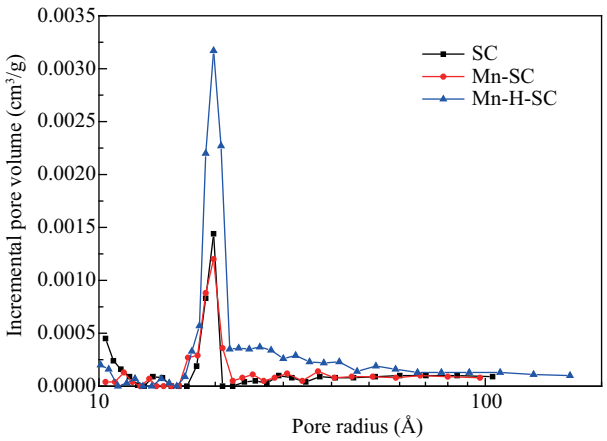

Fig. 2 BJH pore volume range of SC, Mn-SC and Mn-H-SC.

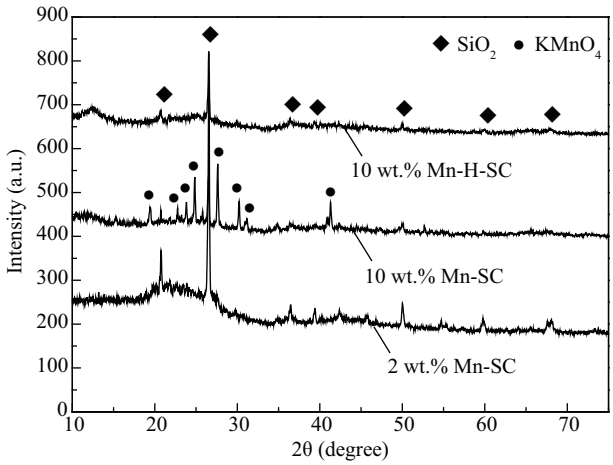

Fig. 3 XRD spectra of Mn-SC and Mn-H-SC.

2.3 X-ray photoelectron spectroscopy

X-ray photoelectron spectroscopy (XPS) is a quantitative spectroscopic technique that measures the elemental composition, empirical formula, chemical state and electronic state of the elements that exist within a material. XPS analyses were completed on the raw adsorbents (SC, Mn-SC and Mn-H-SC) and the adsorbents with captured elemental mercury (Hg-Mn-SC and Hg-Mn-H-SC) (Fig. 4). The main elemental constituents of the virgin semi-coke were C, O and N. After modification by $KMnO_4$, the Mn2p peaks centered at 642 and 654 eV, as well as the Mn3p peak centered at 51 eV, proved that manganese compounds had been loaded on the surface of the treated semi-coke.

Because of the similarity of binding energies between Hg4f and Si2p, the Hg4f energy peak could be masked

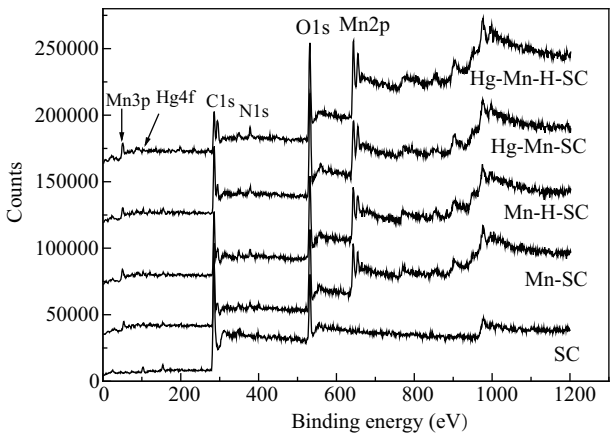

Fig. 4 XPS overall-scan spectra of SC, Mn-SC, Mn-H-SC, Hg-Mn-SC and Hg-Mn-H-SC.

Table 2 Distribution of surface carbon functional groups

Sample	C–C (%)	C–OR (%)	C=O (%)	O=C–OH (%)
SC	51.37	34.32	9.48	4.83
Mn-SC	74.97	12.78	5.22	7.03
Mn-H-SC	75.17	13.40	4.56	6.87
Hg-Mn-SC	77.49	15.58	2.32	4.61
Hg-Mn-H-SC	77.83	14.68	3.21	4.28

by the Si2p energy peak from the semi-coke. Meanwhile, the mercury adsorption capacity of the samples Hg-Mn-SC and Hg-Mn-H-SC was quite low. Therefore, the Hg4f peak at 103.4 eV only could be detected weakly on the surface of the samples Hg-Mn-SC and Hg-Mn-H-SC. Though it was hard to identify the morphology of the adsorbed Hg^0 in the samples, part of the gaseous Hg^0 was definitely adsorbed on the surface of the samples.

Most of the previous studies focused on the relationship between the binding energy of C1s from carbonaceous materials and the structure of chemical functional groups from surface carbon. Zielke et al. (1996) concluded that the relationships between binding energies and carbon functional groups were as follows: C–C–C (284.0–285.1 eV), C–OR (285.3–287.0 eV), C=O (286.8–288.1 eV)and O=C–OH (288.1–290.0 eV). In order to compare the surface functional groups on the samples before and after $KMnO_4$ modification as well as mercury adsorption, XPS Peak Processing software was applied to simulate multi-peaks in the range of C1s and calculate the elemental ratios among different surface carbon functional groups (Table 2).

As shown in Table 2, C–C carbon species were the main carbon components on the surface of SC (51.37%), followed by the carbon species C–OR (34.32%), C=O (9.48%), and O=C–OH (4.83%). $KMnO_4$ modification increased the carbon species of C–C and O=C–OH by 23.6% and 2.2%, and reduced the carbon species of C–OR and C=O by 21.54% and 4.26%, respectively. After the thermal treatment of the sample Mn-SC, no significant change was observed for the carbon species, which indicated that thermal treatment had no influence on the carbon-based functional groups and species. Compared with samples Mn-SC and Mn-H-SC, the mercury adsorption increased the carbon species of C–C and C–OR on the surface of samples Hg-Mn-SC and Hg-Mn-H-SC, and decreased the carbon species of O=C–OH and C=O. One reason was that O=C–OH and C=O functional groups were reduced by the Hg^0 during the gaseous Hg^0 adsorption (Li et al., 2003).

To study the characteristics of manganese compounds on the surface of semi-coke, narrow zone spectrum analysis was carried out for the Mn element. However, the electron binding energies of Mn^{2+}, Mn^{3+}, and Mn^{4+} are so close that the average oxidation state of manganese could not be determined from the Mn2p binding energy. Instead, the $Mn_2p_{3/2}$ spectrum of Mn-SC, Mn-H-SC, Hg-Mn-SC and Hg-Mn-H-SC was fitted with multi-peaks with the parameters of Mn^{7+} (645.6 eV), Mn^{6+} (644.2 eV), Mn^{4+} (643.0 eV), Mn^{3+} (642.1 eV), and Mn^{2+} (641.0 eV) (Fig. 5) (Oku, 1995; Nesbitt and Banerjee, 1998; Wang et al., 2010).

The results of $Mn2p_{3/2}$ multi-peak fitting of different samples are shown in Table 3. The average oxidation degree of manganese on the surface of Mn-SC was 3.80, and the percentage of Mn^{7+} was 4.68%. These results indicated that the potassium permanganate decomposed during the modification, and a portion was reduced by the surface organic functional groups or carbons (Dash et al., 2009) also found that potassium permanganate could be reduced into MnO_2 and formed complexes with the organic groups during the process of oxidation of organic compounds by potassium permanganate. After the thermal treatment of Mn-SC at 260°C, the average oxidation degree of manganese was reduced to 3.46. Meanwhile, the energy peak of Mn^{7+} disappeared, the percentage of Mn^{6+}decreased, and the percentages of Mn^{4+}, Mn^{3+} and Mn^{2+} increased. The temperature of this process was higher than that of potassium permanganate self-decomposition, so the potassium permanganate on the surface of Mn-SC was totally decomposed and part of $Mn^{6+}$was reduced. Compared with Mn-SC, the average oxidation degree of manganese on the surface of Hg-Mn-SC was reduced by 0.73, the energy peaks of Mn^{7+} and Mn^{6+} disappeared, the percentage of Mn^{4+} was almost the same, and the percentages of Mn^{3+} and Mn^{2+} increased dramatically. Clearly, Mn^{7+} and Mn^{6+} were reduced by gaseous Hg^0 during the process of adsorption. Likewise, the temperature of this process was higher than that of the modification process, so self-decomposition presumably occurred for Mn^{7+} and Mn^{6+}. Hg^0 reduction and self-decomposition both led to the reduction of the average oxidation degree of manganese. Compared with Mn-H-SC, the average oxidation degree of manganese on the surface of Hg-Mn-H-SC was reduced by 0.38, the energy peaks of Mn^{6+} disappeared, the percentage of Mn^{4+} decreased slightly, and the percentages of Mn^{3+} and Mn^{2+} increased dramatically. Because the temperature of adsorption was lower than that of the thermal treatment of Mn-H-SC, self-decomposition would not take place for the manganese compounds. Thus the reduction of the average oxidation degree of manganese was the result of the reduction of Mn^{6+} and $Mn^{4+}$by the gaseous Hg^0.

The Hg4f spectrum of Hg-Mn-SC and Hg-Mn-H-SC over the range of 95–110 eV was used to study the adsorption morphology of Hg^0 on the surface of modified semi-coke (Fig. 6). Nevertheless, owing to the interference of the Si2p energy peak, the multi-peak fitting analysis could not be carried out in the range of the narrow zone spectrum of Hg4f to determine its morphology. However, according to the Hg4f spectrum, the mercury binding energies of Hg-Mn-SC and Hg-Mn-H-SC were 103.26 and 103.30 eV respectively, which were nearly the same as that

Table 3 Distribution of surface Mn ions of Mn-SC, Mn-H-SC, Hg-Mn-SC and Hg-Mn-H-SC

Sample	Mn^{7+} (%)	Mn^{6+} (%)	Mn^{4+} (%)	Mn^{3+} (%)	Mn^{2+} (%)	Mn AOS
Mn-SC	4.68	15.29	33.61	28.45	17.97	3.80
Mn-H-SC	0.00	10.62	35.59	32.57	21.22	3.46
Hg-Mn-SC	0.00	0.00	33.94	39.49	26.57	3.07
Hg-Mn-H-SC	0.00	0.00	32.02	44.10	23.88	3.08

AOS: average oxidation state.

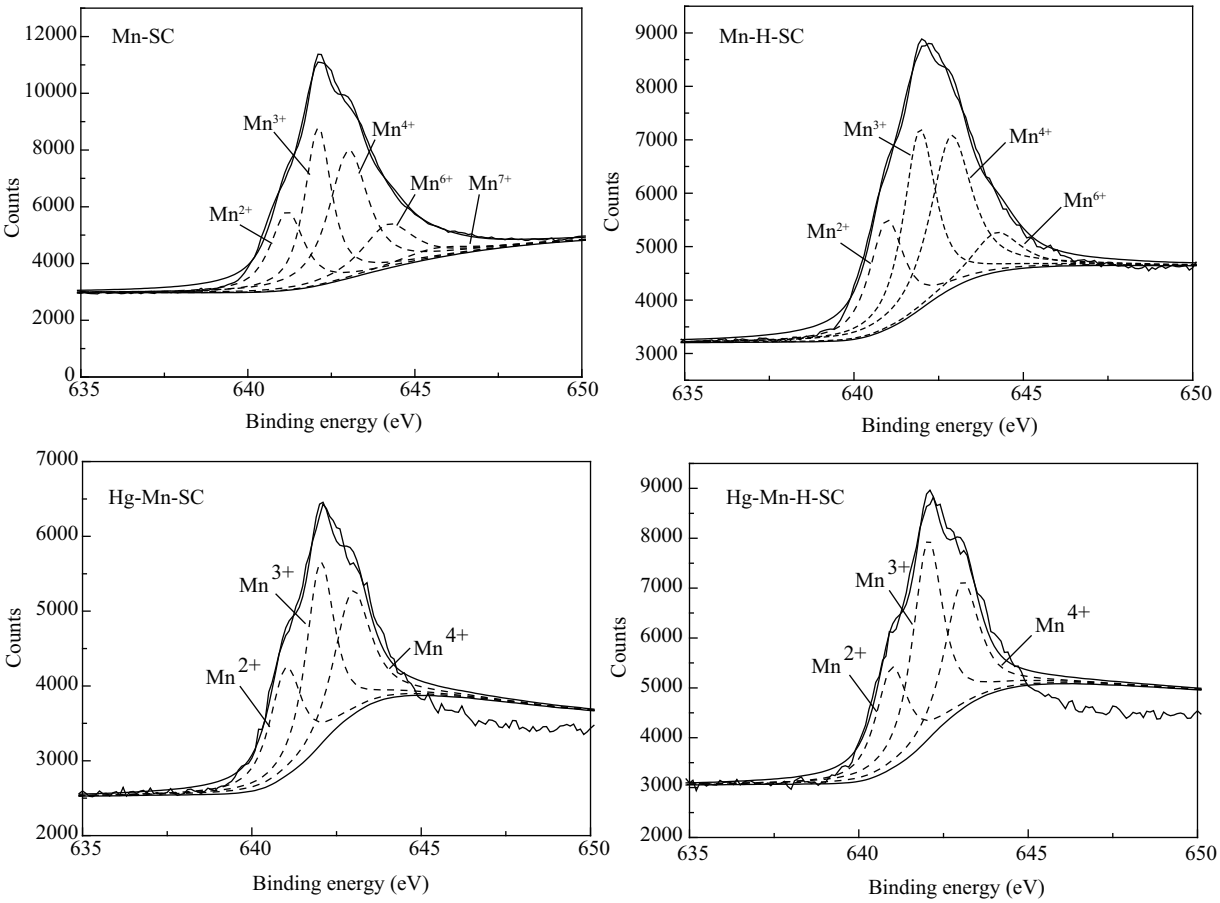

Fig. 5 $Mn2p_{3/2}$ spectrum of Mn-SC, Mn-H-SC, Hg-Mn-SC and Hg-Mn-H-SC.

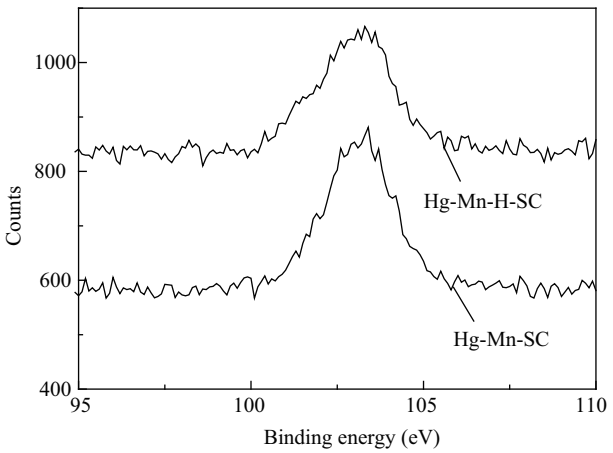

Fig. 6 Hg4f spectrum of Hg-Mn-SC and Hg-Mn-H-SC.

of Hg^{2+} (Behra et al., 2001; Li et al., 2005). No Hg^0 (99.7 eV) (Feng et al., 2006) energy peak was observed. In this sense, mercury existed on the surface of modified semi-coke not in the form of Hg^0, but as Hg^{2+}. More specifically, during the adsorption, the gaseous Hg^0 was first oxidized into Hg^{2+} by MnO_x, and bound with the active adsorption sites which existed on the surface of the modified semi-coke.

2.4 Gaseous Hg^0 removal

Both physical and chemical adsorption contribute to the adsorption of gaseous materials on solid surfaces. The adsorption heat in the process of physical adsorption is low. Therefore, the lower the temperature of adsorption is, the larger the physical adsorption capacity is. By contrast, a large amount of energy is needed during chemical adsorption processes accompanied by electronic transfer or transitions. Thus, the higher the temperature of adsorption, the larger the chemical adsorption capacity. Figure 7 describes the mercury removal efficiencies of SC, Mn-SC and Mn-H-SC at 30, 60, 100 and 140°C, respectively. The mercury removal efficiency of SC decreased as the adsorption temperature was raised (Fig. 7a). When the adsorption temperature increased from 30 to 140°C, the initial mercury removal efficiency and that for 1 hr later decreased from 92.9% and 78.0% to 39.9% and 10.6%, respectively. This suggested that physical adsorption was the main mechanism for mercury adsorption in SC. As the adsorption temperature was raised, the physical adsorption capacity decreased, which resulted in a lower mercury removal efficiency. The mercury removal efficiencies of SC at different adsorption temperatures all decreased as the reaction went on. However, the mercury removal efficiency decreased slowly at lower adsorption temperature, but decreased dramatically at higher adsorption temperature. For instance, after 10 min adsorption of gaseous Hg^0 by SC, the mercury removal efficiencies of the samples at 100°C and 140°C decreased from 89.3% and 39.9% to 51.1% and 16.4%, respectively. SC needs to be modified to increase the mercury removal efficiency at high temperature, since the flue gas from coal-fired utilities is commonly around 120–150°C, under which conditions the

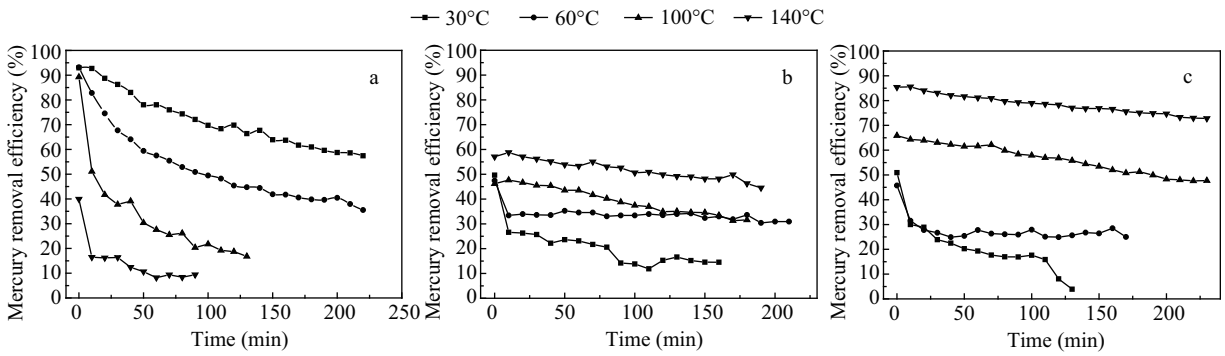

Fig. 7 Mercury removal efficiencies of SC (a), Mn-SC (b) and Mn-H-SC (c) at different temperatures.

mercury removal efficiency of SC is low.

The manganese compounds have good oxidation and catalytic activity, which can oxidize the Hg^0 into Hg^{2+}efficiently. Some researchers loaded MnO_x onto the surface of activated carbon, α-Al_2O_3 and $Ca(OH)_2$, and proved that MnO_x can oxidize Hg^0 and increase the mercury removal efficiencies of the modified samples significantly (Mei et al., 2008; Herranz et al., 2006; Li et al., 2010; Wang and Duan, 2011). The mercury removal efficiency of Mn-SC increased as the adsorption temperature was raised (Fig. 7b). When the adsorption temperature increased from 30°C to 140°C, the initial mercury removal efficiencies and that of 1 hr later increased from 49.7% and 23.6% to 58.8% and 53.3%, respectively. These results suggested that both physical and chemical adsorption contributed to the mercury adsorption in Mn-SC. As the adsorption temperature was raised, the physical adsorption capacity decreased but the chemical adsorption capacity increased, both of which led to higher mercury removal efficiency. Because physical adsorption was the main mechanism for Hg^0 adsorption on the surface of semi-coke at low temperature, the mercury removal efficiency of Mn-SC was much lower than that of SC at low temperature. As presented by the BET data, the surface area and total volume capacity of Mn-SC were lower than those of SC, but the average pore size was a little larger. These properties should be negative for physical adsorption of Hg^0, resulting in low mercury removal efficiencies. Compared with SC, the mercury removal efficiency of Mn-SC was higher at 140°C. In addition, as the adsorption process continued, the mercury removal efficiency decreased much more slowly. The reason for these phenomena was that chemical adsorption mainly contributed to the mercury adsorption at high temperature. The active MnO_x on the surface of Mn-SC oxidized Hg^0 into Hg^{2+} and captured it. The mechanism of this reaction is as follows:

$$Hg(g) \longrightarrow Hg(ad) \quad (2)$$

$$Hg(ad) + MnO_x \longrightarrow HgO + MnO_{x-1} \quad (3)$$

It was the oxidation activity of MnO_x, not the surface area and pore structure, that mainly contributed to the mercury removal efficiency of Mn-SC. The results of XPS showed that the average oxidation degree of manganese on the surface of Mn-SC was high, and the total content of Mn^{7+}, Mn^{6+} and Mn^{4+} reached 53.58%. MnO_x was reduced by the Hg^0 during the adsorption, which led to the decrease of the average manganese oxidation degree and the disappearance of Mn^{7+} and Mn^{6+}.

The mercury removal efficiency of Mn-H-SC also increased as the adsorption temperature was raised, which meant that physical adsorption mainly contributed to the mercury adsorption at low temperature, and chemical adsorption mainly contributed to the mercury adsorption at high temperature (Fig. 7c). Although the surface area and total pore volume of Mn-H-SC were larger than that of Mn-SC, the surface micropore proportion of Mn-H-SC was smaller than that of Mn-SC. As reported, if the diameter of the adsorbent pores is close to the equivalent diameter of adsorbate molecules, the molecular sieve effect would occur to significantly enhance the adsorption capacity of the solid adsorbent when physical adsorption is the dominant mechanism for gas adsorption on the surface (Dubinin, 1989). With an equivalent diameter of 0.157 nm, Hg^0 is mainly adsorbed by the micropores on the surface of semi-coke. Therefore, both the micropore number and the pore structure determine the gaseous Hg^0 adsorption efficiency of semi-coke. The micropore volume (pore size 0.15–0.16 nm) of Mn-H-SC was close to that of Mn-SC, so the mercury removal efficiencies of Mn-H-SC and Mn-SC were almost the same at 30 or 60°C. As the adsorption temperature increased to 100 and 140°C, the mercury removal efficiencies of Mn-H-SC were higher than those of Mn-SC by 20% and 28%, respectively. Compared with Mn-SC, the thermal treatment decreased the average oxidation degree of manganese, Mn^{7+} disappeared, and Mn^{6+} decreased. It appeared that potassium permanganate and partial potassium manganate on the surface of Mn-H-SC decomposed during the thermal treatment, which resulted in the formation of smaller but higher activity amorphous MnO_x micro particles. Though the average oxidation degree of manganese decreased, the micro MnO_x particles highly enhanced the oxidation activity as a whole, which contributed to the higher mercury removal efficiency of Mn-H-SC compared to Mn-SC at high temperature.

3 Conclusions

Chemical modification has great influence on the properties of semi-coke. Compared with the raw sample SC, Mn-SC and Mn-H-SC had much smaller specific surface area, total pore volume and micropore proportion.

The MnO_x was distributed on the surface of Mn-SC

and Mn-H-SC in an amorphous form in low concentration potassium permanganate solution. As the solution concentration increased, crystalline potassium permanganate might precipitate on the surface of Mn-SC. However, because of the decomposition of potassium permanganate during the thermal treatment, MnO_x existed on the surface of Mn-H-SC in an amorphous form.

Chemical modification not only increased the graphitization degree of the semi-coke and the O=C–OH carbon species, but also decreased the carbon species C–OR and C=O. The average oxidation degrees of manganese on the surface of Mn–SC and Mn-H-SC decreased during the adsorption of Hg^0, after which Mn^{7+} and Mn^{6+} disappeared accompanied by the oxidation of Hg^0 to Hg^{2+}.

Physical adsorption was the main mechanism for Hg^0 adsorption on the surface of Mn-SC and Mn-H-SC at low temperature, while chemical adsorption was the main mechanism at high temperature. Generally, thermal treatment can notably improve the mercury removal efficiency of Mn-SC at high temperature. The amorphous MnO_x particles were the active surface oxidation sites for gaseous Hg^0, which contributed to the higher mercury removal efficiency of Mn-H-SC compared to that of Mn-SC at high temperature.

Acknowledgments

This work was supported by the National Natural Science Foundation of China (No. 21006059) and the Project of Shandong Province Higher Educational Science and Technology Program (No. J11LB61).

References

Behra P, Bonnissel-Gissinger P, Alnot M, Revel R, Ehrhardt J J, 2001. XPS and XAS study of sorption of Hg(II) onto pyrite. *Langmuir*, 17(13): 3970–3979.

Bolger P T, Szlag D C, 2002. An electrochemical system for removing and recovering elemental mercury from a gas stream. *Environmental Science & Technology*, 36(20): 4430–4435.

Dash S, Patel S, Mishra B K, 2009. Oxidation by permanganate: Synthetic and mechanistic aspects. *Tetrahedron*, 65(4): 707–739.

Dubinin M M, 1989. Fundmentals of the theory of adsorption in micropores of carbon adsorbents: Characteristics of their adsorption properties and microporous structures. *Carbon*, 27(3): 457–467.

Feng W G, Borguet E, Vidic R D, 2006. Sulfurization of a carbon surface for vapor phase mercury removal(II): Sulfer forms and mercury uptake. *Carbon*, 44(14): 2998–3004.

Gálvez M E, Boyano A, Lázaro M J, Moliner R, 2008. A study of the mechanisms of NO reduction over vanadium loaded activated carbon catalysts. *Chemical Engineering Journal*, 144(1): 10–20.

Gatica J M, Vidal H, 2010. Non-cordierite clay-based structured materials for environmental applications. *Journal of Hazardous Materials*, 181(1-3): 9–18.

Herranz T, Rojas S, Ojeda M, Perez-Alonso F J, Tefferos P, Pirota K et al., 2006. Synthesis, structural features, and reactivity of Fe-Mn mixed oxides prepared by microemulsion. *Chemistry of Materials*, 18(9): 2364–2375.

Hower J C, Senior C L, Suuberg E M, Hurt R H, Wilcox J L et al., 2010. Mercury capture by native fly ash carbons in coal-fired power plants. *Progress in Energy and Combustion Science*, 36(4): 510–529.

Hsi H, Rood M J, Abadi M R, Chen S, Chang R, 2001. Effects of sulfur impregnation temperature on the properties and mercury adsorption capacities of activated carbon fibers (ACFs). *Environmental Science & Technology*, 25(13): 2785–2791.

Hutson N D, Attwood B C, Scheckel K G, 2007. XAS and XPS characterization of mercury binding on brominated activated carbon. *Environmental Science & Technology*, 41(5): 1747–1752.

Jurng J, Lee T G, Lee G W, Lee S J, Kim B H, Seier J, 2002. Mercury removal from incineration flue gas by organic and inorganic adsorbents. *Chemosphere*, 47(9): 907–913.

Lee S J, Seo Y C, Jurng J, Lee G L, 2004. Removal of gas-phase elemental mercury by iodine- and chlorine-impregnated activated carbons. *Atmosphere Environment*, 38(29): 4887–4893.

Lee S S, Lee J Y, Keener T C, 2009. Mercury oxidation and adsorption characteristics of chemically promoted activated carbon sorbents. *Fuel Processing Technology*, 90(10): 1314–1318.

Li H X, Xu Q J, Zhang D Q, 2011. Research on the preparation of silver-loaded semi-coke and its adsorption characteristics to gas-phase Hg^0. *Advanced Materials Research*, 356-360: 1350–1355.

Li J F, Yan N Q, Qu Z, Qiao S H, Yang S J, Guo Y E et al., 2010. Catalytic oxidation of elemental mercury over the modified catalyst Mn/α-Al_2O_3 at lower temperatures. *Environmental Science & Technology*, 44(1): 426–431.

Li N, Bai R B, Liu C K, 2005. Enhanced and selective adsorption of mercury ions on chitosan beads grafted with polyacrylamide via surface initiated atom transfer radical polymerization. *Langmuir*, 21(25): 11780–11787.

Li Y H, Lee C H, Gullett B K, 2003. Importance of activated carbon's oxygen surface functional groups on elemental mercury adsorption. *Fuel*, 82(4): 451–457.

Mei Z J, Shen Z M, Zhao Q J, Wang W H, Zhang Y J, 2008. Removal and recovery of gas-phase element mercury by metal oxide-loaded activated carbon. *Journal of Hazardous Materials*, 152(2): 721–729.

Nesbitt H W, Banerjee D, 1998. Interpretation of XPS Mn(2p) spectra of Mn oxyhydroxides and constraints on the mechanism of MnO_2 precipitation. *American Mineralogist*, 83(3-4): 305–315.

Oku M, 1995. X-ray photoelectron spectra of $KMnO_4$ and K_2MnO_4 fractured in situ. *Journal of Electron Spectroscopy and Related Phenomena*, 74(2): 135–148.

Pirrone N, Cinnirella S, Feng X, Finkelman R B, Friedli H R, Leaner J et al., 2010. Global mercury emissions to the atmosphere from anthropogenic and natural sources. *Atmospheric Chemistry and Physics*, 10(13): 5951–5964.

Presto A A, Granite E J, 2006. Survey of catalysts for oxidation of mercury in flue gas. *Environmental Science & Technology*, 40(18): 5601–5609.

Shangguan J, Li Z L, Li C H, 2005. Investigation on activated semi-coke desulfurization. *Journal of Environmental Sciences*, 17(1): 91–94.

Sundseth K, Pacyna J M, Pacyna E G, Munthe J, Belhaj M, Astrom S, 2010. Economic benefits from decreased mercury emissions: projection for 2020. *Journal of Cleaner Production*, 18(4): 386–394.

Wang D P, Chen H, Du F, Bie X F, Liu L N, Wei Y J et al., 2010. Comparative studies on structure and electronic properties between thermal lithiated $Li_{0.5}MnO_2$ and $LiMn_2O_4$. *Chemical Research in Chinese University*, 26(2): 283–286.

Wang J W, Yang J L, Liu Z Y, 2010. Gas-phase elemental mercury capture by a V_2O_5/AC catalyst. *Fuel Processing Technology*, 91(6): 676–680.

Wang Y J, Duan Y F, 2011. Effect of manganese ions on the structure of $Ca(OH)_2$ and mercury adsorption performance of $Mn^{x+}/Ca(OH)_2$ composites. *Energy & Fuels*, 25(4): 1553–1558.

Yuan M J, Tong S T, Zhao S Q, Jia C Q, 2010. Adsorption of polycylic aromatic hydrocarbons from water using petroleum coke-derived porous carbon. *Journal of Hazardous Materials*, 181(1-3): 1115–1120.

Zielke U, Hültinger K J, Hoffman W P, 1996. Surface-oxidized carbon fibers: I. Surface structure and chemistry. *Carbon*, 34(8): 983–998.

JOURNAL OF ENVIRONMENTAL SCIENCES

(http://www.jesc.ac.cn)

Aims and scope

Journal of Environmental Sciences is an international academic journal supervised by Research Center for Eco-Environmental Sciences, Chinese Academy of Sciences. The journal publishes original, peer-reviewed innovative research and valuable findings in environmental sciences. The types of articles published are research article, critical review, rapid communications, and special issues.

The scope of the journal embraces the treatment processes for natural groundwater, municipal, agricultural and industrial water and wastewaters; physical and chemical methods for limitation of pollutants emission into the atmospheric environment; chemical and biological and phytoremediation of contaminated soil; fate and transport of pollutants in environments; toxicological effects of terrorist chemical release on the natural environment and human health; development of environmental catalysts and materials.

For subscription to electronic edition

Elsevier is responsible for subscription of the journal. Please subscribe to the journal via http://www.elsevier.com/locate/jes.

For subscription to print edition

China: Please contact the customer service, Science Press, 16 Donghuangchenggen North Street, Beijing 100717, China. Tel: +86-10-64017032; E-mail: journal@mail.sciencep.com, or the local post office throughout China (domestic postcode: 2-580).

Outside China: Please order the journal from the Elsevier Customer Service Department at the Regional Sales Office nearest you.

Submission declaration

Submission of an article implies that the work described has not been published previously (except in the form of an abstract or as part of a published lecture or academic thesis), that it is not under consideration for publication elsewhere. The submission should be approved by all authors and tacitly or explicitly by the responsible authorities where the work was carried out. If the manuscript accepted, it will not be published elsewhere in the same form, in English or in any other language, including electronically without the written consent of the copyright-holder.

Submission declaration

Submission of the work described has not been published previously (except in the form of an abstract or as part of a published lecture or academic thesis), that it is not under consideration for publication elsewhere. The publication should be approved by all authors and tacitly or explicitly by the responsible authorities where the work was carried out. If the manuscript accepted, it will not be published elsewhere in the same form, in English or in any other language, including electronically without the written consent of the copyright-holder.

Editorial

Authors should submit manuscript online at http://www.jesc.ac.cn. In case of queries, please contact editorial office, Tel: +86-10-62920553, E-mail: jesc@263.net, jesc@rcees.ac.cn. Instruction to authors is available at http://www.jesc.ac.cn.

Copyright

JOURNAL OF ENVIRONMENTAL SCIENCES

Journal of Environmental Sciences (Established in 1989)
Vol. 24 No. 12 2012

Supervised by	Chinese Academy of Sciences	**Published by**	Science Press, Beijing, China
Sponsored by	Research Center for Eco-Environmental		Elsevier Limited, The Netherlands
	Sciences, Chinese Academy of Sciences	**Distributed by**	
Edited by	Editorial Office of Journal of	Domestic	Science Press, 16 Donghuangchenggen
	Environmental Sciences (JES)		North Street, Beijing 100717, China
	P. O. Box 2871, Beijing 100085, China		Local Post Offices through China
	Tel: 86-10-62920553; http://www.jesc.ac.cn	Foreign	Elsevier Limited
	E-mail: jesc@263.net, jesc@rcees.ac.cn		http://www.elsevier.com/locate/jes
Editor-in-chief	Hongxiao Tang	**Printed by**	Beijing Beilin Printing House, 100083, China

CN 11-2629/X **Domestic postcode: 2-580** **Domestic price per issue RMB ¥ 110.00**

ISSN 1001-0742